The optimization of gamma spectra processing in prompt gamma neutron activation analysis (PGNAA)

Jean-Louis Pinault[1], José Solís[2,*]

[1] IAEA Expert, 96 rue du Port David, 45370 Dry, France
[2] Instituto Peruano de Energía Nuclear, Av. Canadá 1470, San Borja, Lima 41, Perú

Resumen

La incertidumbre del análisis elemental es uno de los factores determinantes para utilizar en línea el análisis por activación de gammas inmediatos (PGNAA) en procesos productivos. En este articulo, se presenta un método general aplicable al procesamiento de un espectro Gamma y aplicado a PGNAA en la industria minera. Este método esta basado en la transformada de Fourier del espectro y su correlación en el espacio Fourier y el procesamiento del solapamiento de los picos característicos minimiza la propagación de errores aleatorios, lo cual optimiza la exactitud y disminuye los límites de detección de los análisis elementales. La mejora puede ser considerable en comparación con el método clásico que se basa en la combinación lineal de las regiones relevantes del espectro, especialmente cuando hay varios elementos que interfieren. El método ha sido aplicado a algunos casos.

Abstract

The uncertainty of the elemental analysis is one of the major factors governing the utility of on-line prompt gamma neutron activation analysis (PGNAA) in the blending and sorting of bulk materials. In this paper, a general method applicable to Gamma spectra processing is presented and applied to PGNAA in mineral industry. Based on the Fourier transform of spectra and their de-correlation in the Fourier space, processing of overlapping of characteristic peaks minimizes the propagation of random errors, which optimizes the accuracy and decreases the detection limits of elemental analyses. In comparison with classical methods based on the linear combinations of relevant regions of spectra the improvement may be considerable, especially when several elements are interfering. The method is applied to four case histories covering both borehole logging and on-line analysis on conveyor belt of raw materials.

1. Introduction

The prompt gamma neutron activation analysis (PGNAA) method has developed considerably for bulk-materials analysis. Taking advantage of the representativity of PGNAA owing to the large mass of material investigated, companies have built commercial systems for the real-time analysis of materials for raw mix preparation [1] such as phosphate [2], limestone, marls and clays intended to the fabrication of clinker [3-8] and coal moving on conveyor belts [9].

In the cement industry, PGNAA enables the optimal blending of raw materials before processing and the verification of chemical uniformity of the final product. In the coal industry, on-line measurements have found particular use in reporting the thermal energy and sulphur content of coal and for determining the fraction of the coal that is not hydrocarbon and will remain as ash after combustion.

In mineral industry, another important industrial application of PGNAA is borehole logging for both the delineation of ore deposits and the in-situ determination of ore quality [10-13]. Borehole logging is a valuable addition for mine exploration and mapping, enabling an automatic real-time update of the mine plan. It can be calibrated to analyze a wide variety of raw materials such as iron, nickel or copper ore, coal or limestone. Borehole logging has mainly developed in open pit coal mines for the determination of ash content as well as in-situ assaying of iron and sulphur. Borehole logging in blast holes produces a representative analysis of the bulk material before being processed.

* Corresponding author: jsolis@ipen.gob.pe

Due to both industrial constrains and the needs for high efficiency detectors, scintillators are generally used for performing Gamma spectrometry. Spectra processing is crucial since the best accuracy has to be obtained in the analysis of raw materials while the strength of the neutron source is as low as possible and the sampling rate is high: typically, measurements occur every minute in process control.

Here is presented a method for spectra processing that minimizes the propagation of random errors in order to optimize the accuracy and to decrease the detection limits of elemental analyses. The bases of this method were presented previously [14] relies on the processing of spectra in the Fourier space. Indeed, this technique has three advantages:

- The peaks and background can be separated easily without modelling background as it is generally required in the physical space. Background may therefore be high, especially when isotopic neutron sources are used, due to neutron interactions into the scintillators.
- The characteristic spectra associated to elements can be de-correlated in order to decrease random errors related to peak area.
- Peak search may be performed in the Fourier space by using an autoregressive filer.

It will be shown the accuracy obtained from this method is close to an optimum from case histories for which the International Atomic Energy Agency (IAEA) backed up the technical part of the projects.

2. The lowest random errors related to peak areas

When the only interference with the characteristic peaks of a given element is background, the lowest relative variance of peak areas referring to a particular element is given by (1).

$$Var = \inf\left[\sum_{n=1,N}\sum_{i=i_1(n)}^{i_2(n)} E(S(i)) \Big/ \left(\sum_{n=1,N}\sum_{i=i_1(n)}^{i_2(n)} \left(E(S(i)) - Bkg(i)\right)\right)^2\right] \quad (1)$$

where *E(S(i))* represents the expected values of the spectrum. The lowest variance is reached by optimizing the boundaries $i_1(n)$ and $i_2(n)$ from which peak areas are integrated. In this relationship it is assumed the main random errors come from counting (2) and (3) and the background *Bkg(i)* is known exactly.

$$Var[S(i)] = E[S(i)] \quad (2)$$

$$Cov[S(i), S(j)] = 0 \; if \; i \neq j \quad (3)$$

The relationship (2) expresses the variance of *S(i)* equals its expected value since it follows a Poisson law and the relationship (3) expresses the independency of *S(i)* and *S(j)*. An estimator of the lowest relative variance of peak areas is obtained by replacing *E(S(i))* by *S(i)* in (1).

Interferences inducing the overlapping of peaks produced by different elements increase the relative variance assigned to the sum of peak areas relative to every elements. The increase in the relative variance is all the more significant as the elementary spectra are correlated. The method that is proposed allows minimizing the relative variance of peak areas that is close to its lowest value (1) when an element is free of interference. When interferences occur between elements the propagation of errors is optimized while overlapping is processed.

3. The determination of peak areas

As was developed in [14] the transformation of spectra in the Fourier space requires a re-sampling of the spectrum so that in the new representation the full width at half maximum (FWHM) is independent of energy. Thus, a step by step integration is used, consisting in using a virtual ADC whose conversion gain for energy *ih* is $\Delta_0 / \Delta(ih)$, where $\Delta(ih)$ is the FWHM at energy *ih* and Δ_0 a constant such as $\Delta_0 \leq \Delta(ih) \; \forall i$ (*h* is the energy increment per channel).

By construction, after re-sampling the spectrum is such that:

- peak areas are preserved;
- the FWHM is Δ_0 independent of the channels.

Moreover, the re-sampling of the spectrum does not alter the relationships (2) and (3). To keep the spectrum clear of discontinuities, it is arranged symmetrically on both sides of the ordinate axis, i.e. the first channel in the

selected window of the spectrum. Thus, the spectrum is defined such that *S(-i) = S(i)*. The Fourier transform (FT) of such a spectrum is real. These precautions are needed to benefit in the Fourier representation from a broad band representative of peaks (discontinuities would generate high frequencies interfering with those characteristic of the peaks).

Peak areas can be estimated by the least squares method which consists in fitting the spectrum represented in the Fourier space by a linear combination of elementary spectra obtained from the detection of unscattered and scattered γ rays issuing from prompt and delayed nuclear reactions. An additional component represents the background produced by unscattered and scattered γ rays issuing from the neutron source as well as neutron interactions into the scintillators. These assertions assume that the spectra can always be restored by a linear combination of such components, which is generally the case in a broad band of the FT. At high frequencies, random errors related to the FT are large. Approximately, random errors generate a white noise in Fourier representation while the FT of peaks strongly decreases when frequencies are increasing. This suggests that a band as representative of the peaks as possible must be selected in the FT of the spectrum. The FT can be written in matrix notation as:

$$\mathrm{FT}(\mathbf{S}) = \mathbf{S}.\mathbf{M} \qquad (4)$$

where $\mathbf{S} = |S(1)\cdots S(N)|$ is the spectrum and ***M*** is a square matrix the general term of which is

$$\phi_{km} = \exp(-2i\pi km/N) \qquad (5)$$

Then, the variance matrix of

$$\mathrm{FT}(\mathbf{S}) = \mathbf{Z} = \mathbf{M}^{*}\mathrm{VAR}(\mathbf{S})\mathbf{M} \qquad (6)$$

where ***M**** is the adjoin matrix of ***M*** and $\mathrm{VAR}(\mathbf{S})$ is the variance matrix of ***S***, the general term of which is $S(k)\delta_{km}$, $\delta_{km} = 1$ if $k=m$ and $\delta_{km} = 0$ if $k \neq m$, from (2) and (3).

Then, the general term of Z is:

$$z_{km} = \sum_{j=0,N-1} S(j)e^{-2i\pi(m-k)j/N} \qquad (7)$$

Therefore, z_{km} is the discrete FT of the spectrum ***S*** at the point $(k-m)/N$. In addition, z_{km} is a Toeplitz matrix i.e. the general term z_{km} depends on the difference $k-m$ of the indices *k* and *m*.

The least squares method consists in minimization of the quadratic sum $R^T Z^{-1} R$ where R is an $(r \times 1)$ column vector of residuals, *r* is the width of the selected band in $\mathrm{FT}(\mathbf{S})$. The elements of R are:

$$r_i = x(i) - \sum_{k=1,p} \theta_k \varphi_k(i) \qquad (8)$$

where *x* is the Fourier transform of the spectrum S, $\varphi_k(i)\ k = 1,\cdots,p$ represent the Fourier transform of the *p* elements. $\mathbf{Z}^{-1}$ is the so-called weight matrix of the observations, **Z** being inverted from the Levinson algorithm. The solution obtained from the weighted least squares method is [14]:

$$\mathbf{\Theta} = \left(\mathbf{\Phi}^T \mathbf{Z}^{-1} \mathbf{\Theta}\right)^{-1} \mathbf{\Theta}^T \mathbf{Z}^{-1} \mathbf{X} \qquad (9)$$

$\mathbf{\Theta}$ is the $(p \times 1)$ column vector whose elements are peak areas θ_k, X is the $(r \times 1)$ column vector whose elements are $x(i)$, i.e. the Fourier transform of S corresponding to the band, $\mathbf{\Phi}$ is an $(r \times p)$ matrix whose elements are $\varphi_k(i)$, i.e. the Fourier transform of the p elementary spectra. The variance of $\mathbf{\Theta}$ is:

$$\mathrm{VAR}(\mathbf{\Theta}) = \left(\mathbf{\Theta}^T \mathbf{Z}^{-1} \mathbf{\Theta}\right)^{-1} \qquad (10)$$

The diagonal terms, i.e. the variance of peak areas, θ_k, strongly depends on the conditioning of the matrix in the second member of (10). This variance can be minimized by selecting a relevant band in the Fourier space in order to de-correlate the Fourier transform of elementary spectra.

4. The de-correlation of elementary spectra in the Fourier space

Due to the Gaussian asymptotic behaviour of peaks, $f(s) = E(\mathrm{FT}(S))$ tends towards:

$$f(s) \rightarrow 2\exp(-2\pi^2\sigma^2 s^2) \sum_{i=1,p} \theta_i \cos(2\pi\pi_i s) \qquad (11)$$

as $|s|$ increases [14]; θ_i is the area of peak i, x_i is its location in S and $\sigma = \Delta_0 / 2\sqrt{2\ln(2)}$ as defined above. If equation (11) represents the Fourier transform $f(s)$ of an elementary spectrum,

the correlation coefficient between two elementary spectra depends on the band $[s_l, s_h]$ on which are defined *f(s)*. Owing to the decreasing of *f(s)*, the influence of the band width is mainly perceptible when the lower limit s_l of spectra in the Fourier space is altered provided the upper limit s_k is large enough. Actually, s_k is fixed to 128 and s_l varies between 1 and 32 (the sampling step of the Fourier transform is $1/64\Delta_0$). In (11) the decreasing term $\exp(-2\pi^2\sigma^2 s^2) = 6.5\,10^{-7}$ if $s = 2/\Delta_0$.

The separation of elementary spectra in the Fourier space $f_i(s)$ and $f_j(s)$ is all the more accurate as the spectra are de-correlated, i.e. the conditioning of the correlation matrix is optimized. For this, their correlation coeficient that depends on the lower limit s_l

$$\frac{\sum_{s=s_l,128}\left(f_i(s)-\overline{f_i(s)}\right)\left(f_j(s)-\overline{j_i(s)}\right)}{\sqrt{\sum_{s=s_l,128}\left(f_i(s)-\overline{f_i(s)}\right)^2}\,x\,\sqrt{\sum_{s=s_l,128}\left(f_j(s)-\overline{f_{ji}(s)}\right)^2}} \quad (12)$$

should be close to 0. The behaviour of the correlation coefficient versus the lower limit s_l of spectra in the Fourier space is illustrated in the last column of Fig. 1 for some couples of elementary spectra obtained from the simulation of prompt γ rays induced by neutron captures. The MOCA Monte Carlo code [15-17] is used with the configuration that corresponds to the on-line analyzer developed in Chile (Table 1, Fig. 2). The simulated spectra represented in the first column of Fig. 1 result from both unscattered and scattered γ rays emitted by the corresponding element. The background is obtained thanks to a benchmark experiment by subtracting the simulated spectra of pure elements from a spectrum obtained experimentally while all the specifications are controlled.

Most of the couples have a zero correlation coefficient provided the lower limit s_l of spectra in the Fourier space is properly defined (last column of Fig. 1). However spectra that are highly correlated in the physical space (the correlation coefficients of the couples (Fe, Al), (Fe, Cu) and (Al, Cu) are 0.70, 0.88 and 0.59, respectively) have correlation coefficients that may not decrease below 0.5 in the Fourier space whatever the lower limit s_l.

In the case of complex spectra S from which the characteristic spectra of n elements have to be separated, suppose the following decomposition:

$$S = \theta_1 S_1 + \cdots + \theta_n S_n + \theta_{Bkg} S_{Bkg} + \varepsilon \quad (13)$$

where $S_1, \cdots, S_n$ are the characteristic spectra, S_{Bkg} is the background and ε represents the noise. The same decomposition is still valid in the Fourier space:

$$FT(S) = \theta_1 FT(S_1) + \cdots + \theta_n FT(S_n) + \theta_{Bkg} FT(S_{Bkg}) + FT(\varepsilon) \quad (14)$$

and, to be separated properly every component S_i has to be de-correlated from the remaining part of the spectrum, i.e.:

$$\theta_1 FT(S_1) + \cdots + \theta_{i-1} S_{i-1} + \theta_{i+1} S_{i+1} + \cdots + \theta_n FT(S_n) + \theta_{Bkg} FT(S_{Bkg}) \quad (15)$$

It is the reason why the random errors related to the concentrations estimated from the peak areas depend on the lower limit s_l of spectra in the Fourier space. Thus, for every element *i*, s_{opt} is optimized while the calibration curves are computed from the general equation (16) the coefficients $\beta_0, \beta_1, \cdots$ being related to the inter-elements effects (q is the number of elements involved in the inter-element effects):

$$\hat{C}_i = \theta_i.\left(\beta_0 + \beta_1\theta_1 + \cdots \beta_q\theta_q\right) \quad (16)$$

Indeed, since the estimated standard deviation *Std*:

$$Std = \frac{1}{N-1}\sqrt{\sum_{i=1,N}\left(C_i - \hat{C}_i\right)^2} \quad (17)$$

that characterizes the deviations between the standards C_i used for the calibration and the estimated concentrations $\hat{C}_i$ (N is the number of samples) depends on the lower limit s_l of spectra in the Fourier space, s_{opt} is defined such that the standard deviation is minimum, i.e.:

$$Std(s_{opt}) = \min_{s_l}\left(std(s_l)\right) \quad (18)$$

The method is illustrated in Fig. 3 for the calibration of the main components of bulk materials that have been analysed within four case histories, i.e. borehole logging in limestone intended to the production of cement (Cementos Lima, Peru), borehole

logging and on-line analysis on conveyor belt of porphyry copper (Chuquicamata mine, Chile) and on-line analysis of ash in coal (steel mill Acerias Paz del Rio, Colombia). The standard deviations versus the lower limits s_l of spectra in the Fourier space are minimized in Fig. 3(a), (g), (m) and (s).

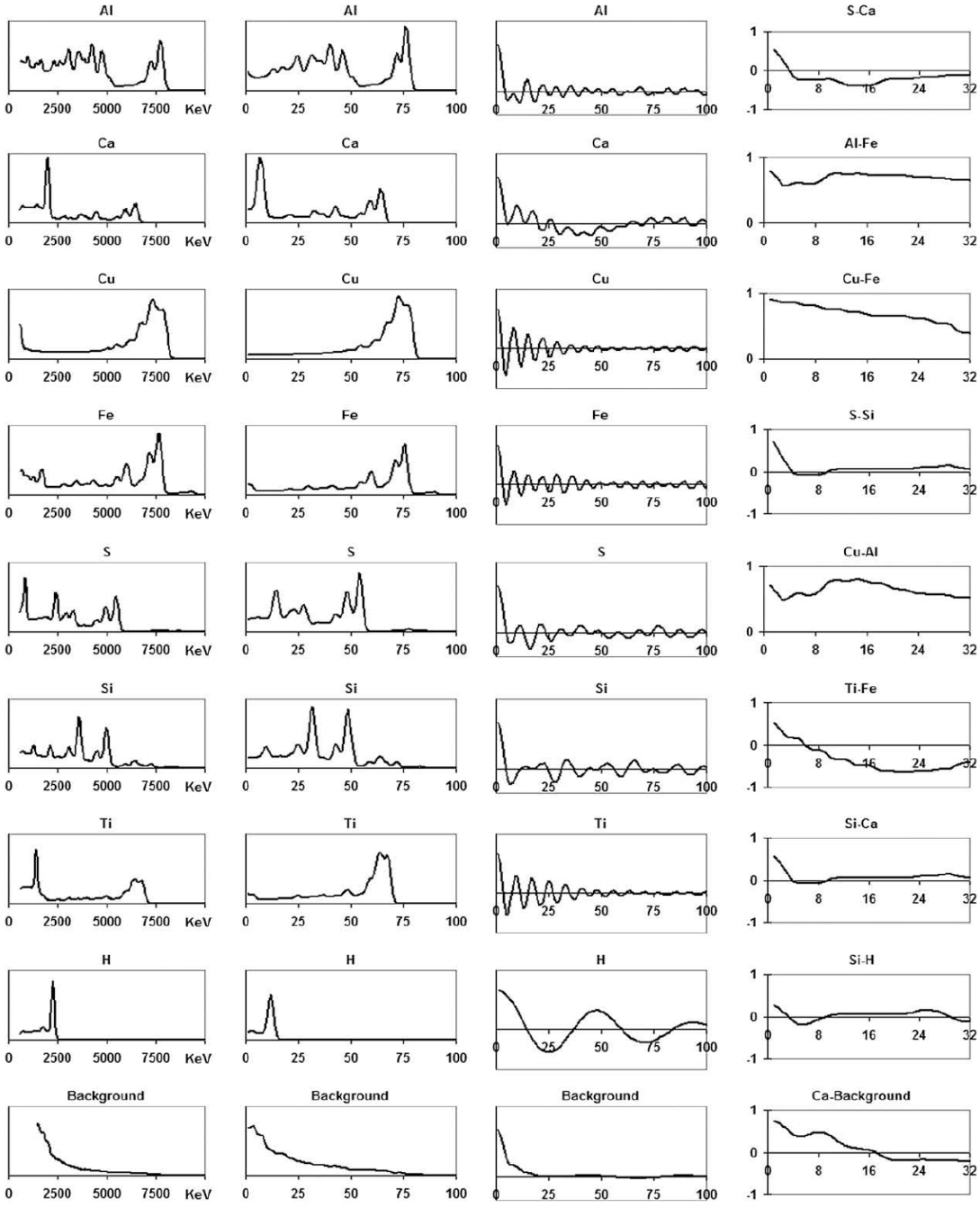

Figure 1. Original and transformed spectra. The first column represents the elementary spectra simulated by Monte Carlo method that are used in the different case histories and the background (count rates represented on Y-axis are arbitrary); a 3 in.x3in. BGO detector used. The second column represents the same spectra once they are resampled. The third column exhibits the Fourier transforms of the re-sampled spectra an the last column shows the correlation coefficient (12) of the Fourier transforms versus the lower limit s_l from which the transformations are considered.

Table 1. Specifications of the equipments.

	Target	Source activity (MgCf)	Size detector BGO	Source to detector spacing (cm)	Resolution (keV for H peak)	Threshold for spectra processing (Mev)	Gain stabilization	Acquisition time (s)	Spectra used for calibration obtained	Number of samples for calibration
Peru borehole logging	Cement	0,45	2 in. x 4 in.	27	198	1,8	Hardware	420	Experimentaly	28
Chile borehole logging	Copper	0,83	2 in. x 4 in.	27	198	1,8	Hardware	750	Experimentaly	54
Chile on-line analyzer	Cooper	9,2	3 in. x 3 in.	61,25	190	1,8	Software	245	Simulated	10
Colombia on-line analyzer	Coal quality	9,3	3 in. x 3 in.	61.25	185	2.4	Software	765	Simulation	7

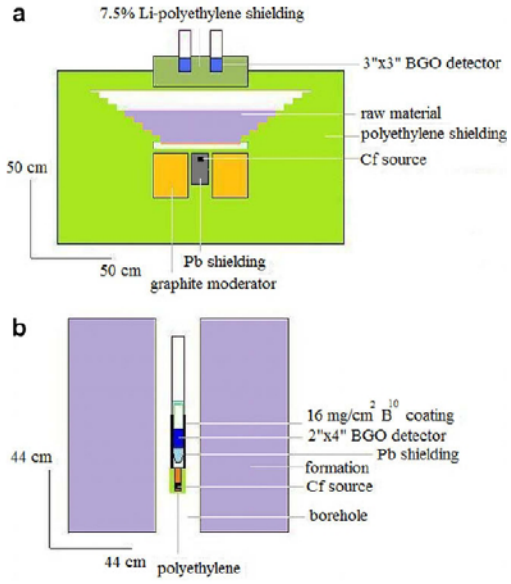

Figure 2. Configurations used in the Monte Carlo code – (a) On-line analyser: 2 detectors are used to improve the representativity of the analysis throughout the cross section of the material. The moderator of neutrons while preventing them from escaping from the analyser. Lithied polyethylene around the detector slows down and absorbs neutrons without emiting spurious γ rays. The contours of the material on the belt reflect the elements used in the Monte Carlo code to take into account the actual geometry of the belt and the shielding- (b) Borehole logging: polyethylene around the source contributes to the termalization of neutrons into the formations the water content of which is low. Boron in the coating around the detector is intended to absorb thermal neutrons while the characteristic peak may be used as an indicator of the thermal neutron flux into the formation. The configurations are the same in Peru and Chile, blast hole diameter except: 24 cm in Chile, 11.2 cm in Peru.

5. The achievement of calibration within the case histories

5.1 Borehole logging of SiO_2, Al_2O_3, Fe_2O_3, $CaCO_3$ and SO_3 in limestone intended to cement production

Due to the frequent handling of the probe, the neutron source used for borehole logging must have a relatively low neutron flux (Fig. 2). Actually, 1 µg Cf sources are frequently used for this purpose (1 µg of Cf^{252} emits 2.3 $x10^6$ n/s). On the other hand, the geometry of the formation around the irradiation system promotes the containment of neutrons, and thermal neutrons are all the more overcrowded in the vicinity of the probe as water content is higher.

Since the main peaks in spectra are issuing from Ca and H (Fig. 4), the de-correlation of elementary spectra mainly concerns Si, Fe, Al and S that exhibit clearly visible minimums (Fig. 3(a)). The calibration curves (Fig. 3(b)-(f)) are obtained from the comparison of peak areas to the analysis of cuttings in laboratory. Most of the discrepancies between borehole logging and the reference analysis are due to sampling errors because both methods do not apply on the same support (what the geostatistician name the support effect) and possibly to a poor recovery of samples. Indeed, the analysis of cuttings or cores concerns the material into the borehole whereas the logging investigates a volume around the borehole that is about ten times higher than a core. Another problem occurs in the calibration due to the variation of neutron flux into the formation owing to the variation of water content and, possibly, to the

presence of neutron poisons such as rare earths. So, the calibration equation has to take into account the action of such disturbing effects on the yield of prompt γ rays. Several techniques may be used to normalize peak areas: the use of the peak of boron produced by the *n*, α reaction when thermal neutrons are absorbed by B^{10} into the coating around the detector (Fig. 2(b)) or the hydrogen peak. The normalization may also be carried out by constraining the sum of the concentration of analysed components to be constant. Here, the sum of the five components remains close to 96% almost everywhere into the quarry, excepted in some particular parts of limestone that underwent metamorphism. Since the present calibration equation does not concern this very particular part of the quarry, the sum of concentrations is constrained in the calibration curves presented in the first column of Fig. 3. The remaining components not analyzed are magnesium carbonate $MgCO_3$ and alkalis.

5.2 Borehole logging of SiO_2, Al_2O_3, Fe_2O_3, SO_3 and Cu in porphyry copper

Here the main peaks are produced by H, Si and Fe (Fig. 4) and, consequently, mainly the calibration curves of Al and Cu are sensitive to the lower limit s_l of spectra in the Fourier space in (18), all the more as the main peaks of the spectra of Fe, Al and Cu are overlapped (Fig. 1). As in the previous case history, the formation is located in an arid area and, consequently, water content is low (a few percent), which is not favourable to the containment of thermal neutrons around the probe. Moreover, fast neutrons that interact with the detector induce a high background. The discrepancies between the reference and the estimated concentrations are mainly due to the support effect (Fig. 3), especially SiO_2, Al_2O_3 and SO_3. In order to take into account inter-element effects along the boreholes peak areas of H, Si and Al are used in the calibration Eq. (16).

5.3 On-line analysis on conveyor belt of SiO_2, Al_2O_3, Fe_2O_3, SO_3 and Cu in porphyry copper

On-line analysis requires higher neutron fluxes because the geometry of the equipment is not favourable to the overcrowding of neutrons into the raw material to be analysed. Therefore, the thickness of the material on the conveyor is generally lower than the free mean path of fast neutrons and both moderator and neutron reflectors are required to increase the yield of γ rays issuing from neutron reactions into the material (Fig. 2). Another specificity of the on-line analysis for process control is the shortness of the sampling rate while the accuracy of analyses determines the efficiency of the control. In the present process the thickness of the material on the belt varies significantly and this disturbing effect is taken into account into the calibration equation from the H peak that reflects the shielding capacity of the material layer. Indeed, the thicker the layer the weaker the H peak produced by neutrons that are absorbed in polyethylene around the detectors.

The calibration is carried out from simulated complex spectra after the source activity and the resolution of detectors were determined from a benchmark experiment for which the composition of the material, its thickness on the conveyor and its density were controlled. Here again, mainly Al and Cu exhibit minimums in Fig. 3(m). showing the estimated standard deviations according to the lower limit s_l of spectra in the Fourier space. Discrepancies between reference and estimated concentrations are lower than in the previous case histories since here the accuracy of Monte Carlo calculations is tightly controlled. The re-sampling of spectra is used for stabilizing the gain of the spectrometer by minimizing the discrepancies between the experimental spectrum and the spectrum reconstructed from the linear combination of elementary spectra, parameter adjustment being the offset and the conversion gain of the virtual ADC.

5.4 On-line analysis on conveyor belt of ash and sulphur in coal

Here again the calibration is achieved from simulated spectra (Fig. 3(s)-(x)). The spectra mainly exhibit H, C, Si and Fe peaks (Fig. 4(g) and (h)). H peak results from the shielding and the volatiles in ash. Carbon peaks are produced both by neutron capture (4.945 Mev) and inelastic scattering of neutrons (4.439 Mev) in coal. Carbon peaks are used for gain stabilization whereas this function was performed from the H peak in

the previous case history. They are also used to take into account the variations of the thickness of coal on the belt. Due to the presence of C peaks in the vicinity of Si, S and Al peaks, the sensitivity of standard deviations to the lower limit s_l of spectra in the Fourier space is outstanding (Fig. 3(s)).

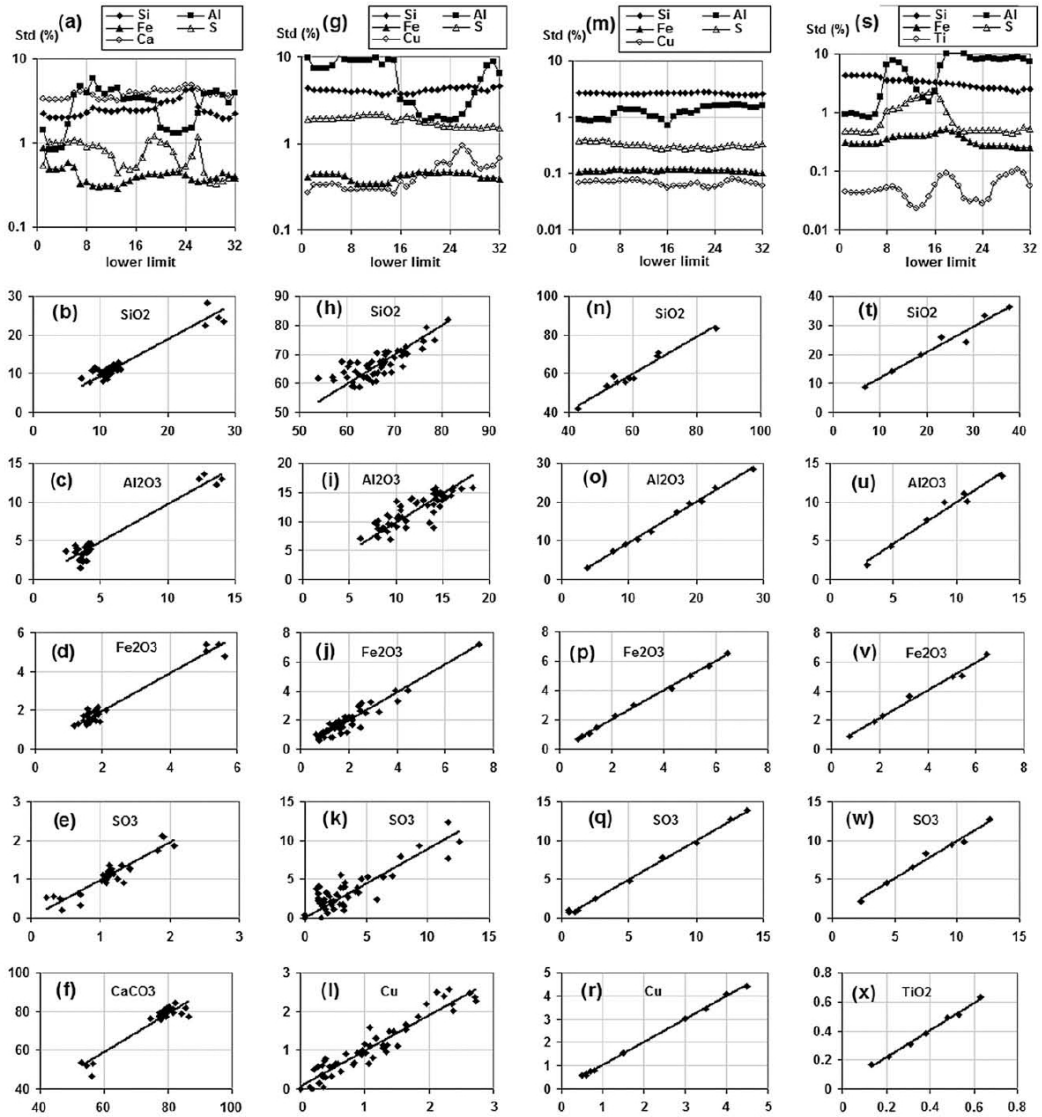

Figure 3. Optimization of the lower limits sl of spectra in the Fourier space. The Four columns are referring to the four case stories, namely borehole logging in limestone (Peru) and in copper ore (Chile), on-line analysis of copper are (Chile) and ash content in coal (Colombia) – (a), (g), (m), (s) the standard deviations versus the lower limit sl of spectra in the Fourier space – (b-f), (h-l), (n-r) and (t-x) the corresponding calibration curves.

6. Results and discussion

In Table 2 are quantified the effective random errors that result from the propagation of Poissonian errors related to the counts when interferences are processed (10). They are compared to the theoretical random errors (1), both being obtained in standard conditions. Effective random errors are much lower than the discrepancies observed for the calibration, which are quantified from the standard deviations at the minimum of the curves in Fig. 3(a), (g), (m), and (s). This observation suggests that the discrepancies mainly reflect systematic errors. Nevertheless, the de-correlation of elementary spectra in the Fourier space

obtained from the lower limit s_l of spectra in the Fourier space that minimizes the standard deviation (18) operates efficiently. Indeed, the effective random errors are hardly higher than the theoretical random errors for Fe_2O_3 and SO_3. When significant overlapping of characteristic peaks occurs, the effective random errors increase in comparison with the theoretical errors, all the more as the overlapping is more severe. In presence of Fe and Cu, the effective errors related to Al_2O_3 may be three times higher than the theoretical errors as occurs for borehole logging in porphyry copper.

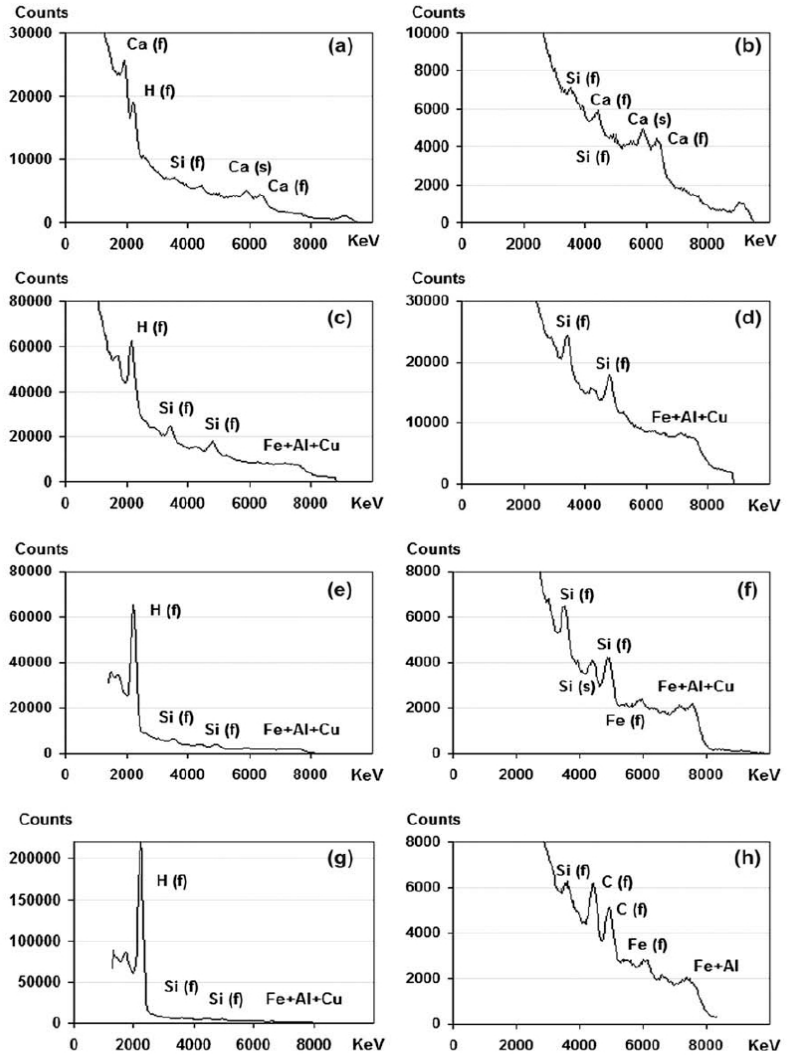

Figure 4. Representative spectra obtained within the four case stories- (a) and (b) borehole logging in limestone, Peru: borehole 489- (c) and (d) borehole logging in porphyry copper, Chile: borehole 2001 – (e) and (f) on-line analysis of porphyry copper, Chile: 11 June 2001 16:16 – (g) and (h) 0n-line anslysis of ash in coal, Colombbia: 19 June 2002 18:38.

Nevertheless, this increase in the random errors is low in comparison with the propagation of errors that occur when classical methods based on the linear combination of relevant regions of the spectrum are used to remove interferences. For example, the effective random error related to Al_2O_3 in ash as shown in Table 2(d) would be 3.12%, i.e. 4 times the theoretical error, if the contribution of Fe in the multiplet resulting from both Fe peaks (7.63 and 7.65 Mev) and Al peak (7.72 Mev) was subtracted by using the Fe peaks at 5.92 and 6.02 Mev that are free of interference (Fig. 4(f)).

Table 2. The standard deviations of concentrations are represented for standard conditions: specifications of the systems are represented in Fig. 2 – (a) and (b) borehole logging with a 1 lg Cf source, acquisition time is 300 s – (c) and (d) on-line analysis with a 20 lg Cf source, acquisition time is 300 s. Theoretical standard deviations are calculated from (1) and the effective standard deviations are calculated from (10).

	SiO_2	Al_2O_3	Fe_2O_3	SO_3	$CaCO_3$
(a)					
Theoretical limit	0,29	0,34	0,04	0,14	0,29
Effective	0,49	0,41	0,09	0,21	0,60
Typical concentration	11	4	2	1	78
	SiO_2	Al_2O_3	Fe_2O_3	SO_3	Cu
(b)					
Theoretical limit	0,45	0,54	0,04	0,22	0,04
Effective	0,72	1,78	0,04	0,27	0,13
Typical concentration	70	10	0,50	2,50	2
	SiO_2	Al_2O_3	Fe_2O_3	SO_3	Cu
(c)					
Theoretical limit	0,42	0,65	0,05	0,22	0,02
Effective	0,55	1,32	0,08	0,26	0,06
Typical concentration	58	10	6	5	3
	SiO_2	Al_2O_3	Fe_2O_3	SO_3	TiO_2
(d)					
Theoretical limit	0,62	0,72	0,04	0,31	0,02
Effective	0,72	0,89	0,04	0,33	0,02
Typical concentration	12	2	1	4	0,20

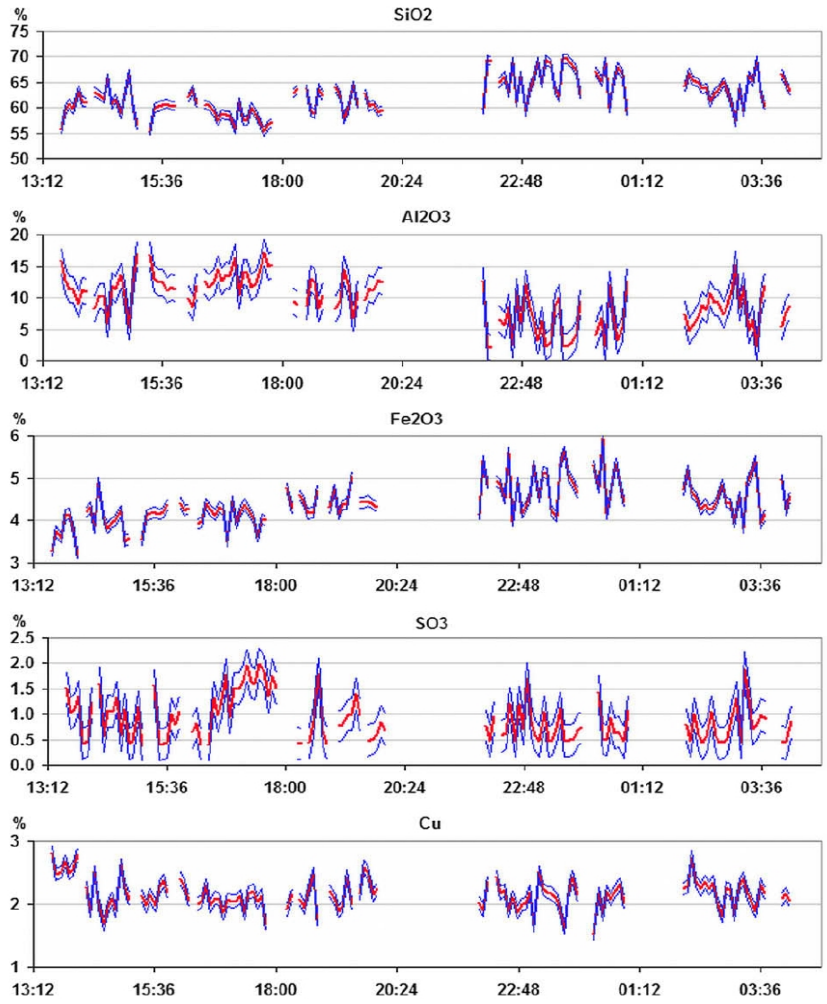

Figure 5. On-line analysis of copper ore in the Chuquicamata mine (Chile, 11–12 June 2001).

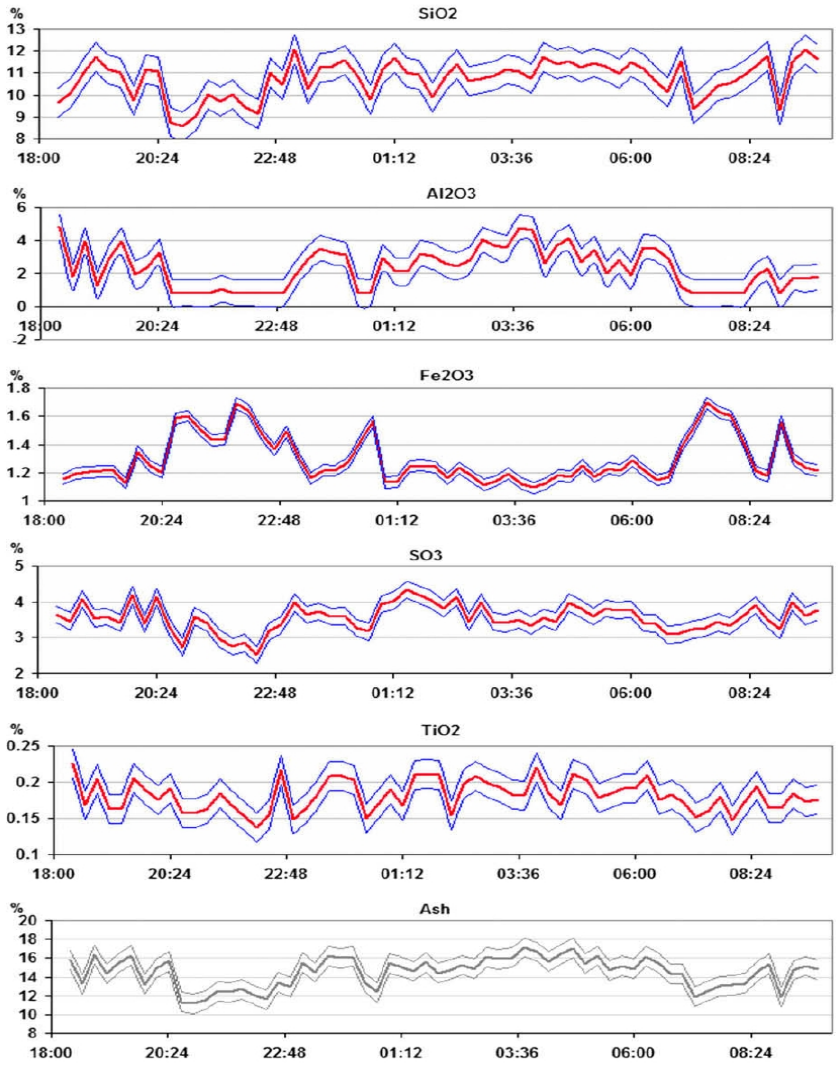

Figure 6. On-line analysis of ash content and sulphur in coal in the steel mill Acerias Paz del Rio (Colombia, 19–20 June 2002).

The application of the method is illustrated in Fig. 5 and Fig. 6 showing sequences of analyses that were performed to demonstrate the feasibility of the on-line analysis of raw materials on conveyor belt while all components of the analyzers are available commercially, which drastically decreases the price of the equipment provided the random errors are minimized to balance the low counting rate.

In Fig. 5 the on-line analysis is performed on a conveyor belt that feeds the beneficiation plant of the Chuquicamata mine and the concentration framed by the standard deviation computed from the propagation of random errors (10) is represented (specifications are shown in Table 1). The standard deviation deduced from the short term variance of the series, i.e.

$\frac{5}{4\mathrm{N}}\sum_{i=1,N}\left(\hat{C}_i-\overline{\hat{C}_i}\right)^2$ where $\overline{\hat{C}_i}$ is the mobile average of the concentration $\hat{C}_i$ (calculated from 5 values) and N is the number of values are represented in Table 3 as well as standard deviations deduced from (10) and calculated for the actual specifications (Table 1). They are not significantly different for Al_2O_3 and SO_3 while the concentrations of SiO_2, Fe_2O_3 and Cu highlights their temporal variability.

In Fig. 6 the on-line analysis of coal is performed on a conveyor belt that feeds the steel mill where the pellets intended to the

blast furnace are prepared. The couples of standard deviations represented in Table 3 show that none of them are significantly different, Fe excepted, which means the accuracy of the analyses mainly allows highlighting long term variability, as shown in Fig. 6. The standard deviations of ash content (the sum of SiO_2, Al_2O_3, Fe_2O_3 and TiO_2) are very close, too, 1.05% and 1.19% for effective and short term random errors, respectively. Actually, the coal has been homogenized before feeding the plant and mainly long term variations in coal quality are relevant for process control at the input of the steel mill.

Table 3. The standard deviations of concentrations are represented for actual conditions (Table 1) as well as the short term standard deviations – (c and d) are referring to the same case stories than in Table 2.

	SiO_2	**Al_2O_3**	**Fe_2O_3**	**SO_3**	**Cu**
(c)					
Effective	0,90	2,15	0,13	0,43	0,10
short term	2,77	2,95	0,43	0,38	0,23
	SiO_2	Al_2O_3	Fe_2O_3	SO_3	TiO_2
(d)					
Efecctive	0,66	0,82	0,04	0,30	0,02
short term	0,77	0,86	0,12	0,30	0,02

7. Conclusions

The method that is proposed to optimize Gamma spectra processing in PGNAA is not new since it has already been presented in [14] and some on-line analyzers are equiped with software based on the separation of elementary spectra in the Fourier space (it seems nothing has yet been published). Nevertheless, some improvements of the method based on the de-correlation of elementary spectra deserve to be known all the more as they allow minimizing the propagation of random errors when multiplets of peaks are separated. This method is valuable for on-line analysis because accuracy determines the efficiency of industrial processes but also for borehole logging to improve accuracy and to allow analysing more elements.

8. Acknowledgments

This work was supported by IAEA projects COL/8/020, CHI 8/024 and PER/1/014. Thanks a lot for the persons who participated actively to the projects: Felipe Mujica, Neida Heresi and Ivan Piñero (Instituto de Innovación en Mineria y Metalurgia SA., Santiago, Chile), Oscar Duran (Comisión Chilena de Energia Nuclear, Santiago, Chile), German Perez, Alberto Bohorques (University of Valle, Cali , Columbia), Jairo Duque (Centro de Investigaciones Nucleare, Bogota, Columbia).

8. References

[1]S. Weiss E. Gartner., IEEE Transactions on Industry Applications. IA-22 (2) (1986) 324.
[2] Douglas S, Darrell L. ISA TECH/EXPO Technology Update Conference Proceedings. 1996; 51(2):1231.
[3] Glorieux G, Lanz V, *et al*. IEEE Cement Industry Technical Conference. (1990) 187.
[4] Tschudin M, Galdeano V, et al. ZKG International, Edition B. 1994;47(3):136.
[5]R. Steven A. IEEE Cement Industry Technical Conference (1997) 433.
[6] Leetham D, Ackermann R. World Cement. 2004; 35(11):85.
[7] Aguilar MO, Ceballos FG, Balboa C. World Cement. 2005; 36(4):17.
[8]S. Banks, M., Edwards, World Cement, 38 (6) (2007) 51.
[9]T. Schade, R. Woodward, Instrumentation in the Mining and Metallurgy Industries 12 (1985) 97.
[10]S.S. Nargawalla, A. Kung, O.J. Legrady, J. Strever, A. Csilag, H.O. Seigel, 1977. Nuclear metalog grade logging in mineral deposits. Proceedings of the IAEA Symposium on Nuclear Techniques, Mineral Resources 1977, Vienna, March 1977, pp. 229.
[11]M. Borsaru M. Berry, M. Biggs, A. Rojc, Nucl. Instr. And Meth. B 213 (2204) 530.
[12]J. Charbucinski, J. Malos, A. Rojc, and C. Smith, Appl. Radiat. Isotopes, 59 (2-3) (2003) 197.
[13]J. Charbucinski and W. Nichols, Appl. Energy, 74 (3) (2003) 313.
[14]J-L Pinault, Nucl. Instr. and Meth. A 305 (1991) 462.
[15] Pinault JL, Gâteau C. Nucl. Geophys. 1989; 3(4):487.
[16] Pinault JL. Nucl. Geophys. 1990; 4(4):443.
[17] Pinault JL. Nucl. Geophys. 1991; 5(3): 229.